

Scalable Superior Chemical Sensing Performance of Stretchable Ionotronic Skin via a π -Hole Receptor Effect

Ming Liang Jin,* Sangsik Park, Hyukmin Kweon, Hyeong-Jun Koh, Min Gao, Chao Tang, Soo-Yeon Cho, Yunpyo Kim, Shuye Zhang, Xinlin Li, Kwanwoo Shin, Aiping Fu, Hee-Tae Jung,* Chi Won Ahn,* and **Do Hwan Kim***

Skin-attachable gas sensors provide a next-generation wearable platform for real-time protection of human health by monitoring environmental and physiological chemicals. However, the creation of skin-like wearable gas sensors, possessing high sensitivity, selectivity, stability, and scalability (4S) simultaneously, has been a big challenge. Here, an ionotronic gas-sensing sticker (IGS) is demonstrated, implemented with free-standing polymer electrolyte (ionic thermoplastic polyurethane, i-TPU) as a sensing channel and inkjet-printed stretchable carbon nanotube electrodes, which enables the IGS to exhibit high sensitivity, selectivity, stability (against mechanical stress, humidity, and temperature), and scalable fabrication, simultaneously. The IGS demonstrates reliable sensing capability against nitrogen dioxide molecules under not only harsh mechanical stress (cyclic bending with the radius of curvature of 1 mm and cyclic straining at 50%), but also environmental conditions (thermal aging from -45 to 125 °C for 1000 cycles and humidity aging for 24 h at 85% relative humidity). Further, through systematic experiments and theoretical calculations, a π -hole receptor mechanism is proposed, which can effectively elucidate the origin of the high sensitivity (up to parts per billion level) and selectivity of the ionotronic sensing system. Consequently, this work provides a guideline for the design of ionotronic materials for the achievement of high-performance and skin-attachable gas-sensor platforms.

Soft, skin-attachable sensing devices have enabled the perception of infinitesimal changes in the surroundings (i.e., pressure and temperature) for intelligent robots, medical diagnostics, and real-time health monitoring.^[1,2] In artificial sensing platforms, additional functionalities for chemical and biological sensing are designed to incorporate and facilitate a high quality of life.^[3,4] Because exposure to toxic chemicals leads to millions of deaths worldwide annually, the use of skin-attachable platforms for sensing toxic gases has attracted considerable attention.^[5] For example, toxic nitrogen dioxide (NO_2) gas molecules from automotive emissions are associated with respiratory mortality and morbidity, thus it must be monitored along with other toxic chemicals.^[6,7]


To realize the practical sensing of toxic gases via skin-attachable devices, the sensor should be designed with long-term stability (chemical, thermal, and mechanical robustness that enable reliable collection of sensing signals on the human

Prof. M. L. Jin
Institute for Future
Automation School of Qingdao University
Qingdao 266071, China
E-mail: jinmingliang@qdu.edu.cn

Prof. M. L. Jin
Shandong Key Laboratory of Industrial Control Technology
Automation School of Qingdao University
Qingdao 266071, China

S. Park
Department of Chemical Engineering
Pohang University of Science and Technology
Pohang 37673, Republic of Korea

H. Kweon, Prof. D. H. Kim
Department of Chemical Engineering
Hanyang University
Seoul 04763, Republic of Korea
E-mail: dhkim76@hanyang.ac.kr

 The ORCID identification number(s) for the author(s) of this article can be found under <https://doi.org/10.1002/adma.202007605>.

H.-J. Koh, Prof. H.-T. Jung
Department of Chemical and Biomolecular Engineering (BK-21 Plus)
Korea Advanced Institute of Science and Technology (KAIST)
Daejeon 305–701, Republic of Korea
E-mail: heetae@kaist.ac.kr

M. Gao
Institute of Microengineering
École Polytechnique Fédérale de Lausanne (EPFL)
Rue de la Maladière 71b, Neuchâtel 2000, Switzerland

Dr. C. Tang
Department of Mechanical Engineering
Tsinghua University
Beijing 100084, China

Dr. S.-Y. Cho
Department of Chemical Engineering
Massachusetts Institute of Technology
77 Massachusetts Avenue, Cambridge, MA 02139, USA

Y. Kim, Prof. K. Shin
Department of Chemistry and Institute of Biological Interfaces
Sogang University
Seoul 04107, Republic of Korea

DOI: 10.1002/adma.202007605

skin), high sensitivity, and selectivity under room-temperature operating conditions. Additionally, to enable low-cost fabrication for feasible large-scale commercialization, the implementation of a printing processing technique (for example, spray-coating, stamping, and inkjet printing) on stretchable substrates is one of the best candidates to replace complex, multistep, conventional optical lithography.^[8] Hence, for reliable signal acquisition in real-life operating environments, the development of skin-attachable gas sensors with high sensitivity, selectivity, stability, and scaled fabrication (parameters collectively known as 4S) is essential.

Chemiresistors are particularly suitable for sensing chemicals because of their flexibilities, high sensitivities, and reversible sensing properties when compared with other traditional detection tools,^[9,10] including gas chromatography-mass spectrometer,^[11] ion flow-tube mass spectrometer,^[12] surface acoustic wave sensors,^[13] and quartz crystal microbalance.^[14] Electrical sensing materials that have been intensively investigated for application in chemiresistors include semiconducting metal oxides,^[15] monolayer-capped metal particles,^[16–18] metal nanowires,^[19] conductive polymers,^[20] carbon nanotubes (CNTs),^[21] and 2D materials.^[22–24] Among these, semiconducting metal oxide materials have been widely used for highly sensitive NO₂ detection; however, to attain high sensitivity, these sensors inevitably require operating temperatures that are too high (200–600 °C) for practical wearable sensors.^[25–28] 2D materials, which include graphene,^[29] transition metal dichalcogenides,^[30] black phosphorus,^[31,32] and Ti₃C₂T_x (MXene),^[33] have also been investigated for highly sensitive NO₂ sensing because of the large number of adsorption sites created by their large surface area-to-volume ratios, but insufficient environmental (temperature, water, and oxygen stability) and mechanical (strain) robustness, and inferior reversible sensing properties still remain as challenges.

Green chemistry materials, such as ionic liquids (ILs), have recently revolutionized multidisciplinary sciences, including chemistry, physics, biology, and engineering, owing to their unique physico-chemical properties.^[34] For example, their characteristics such as extremely low vapor pressure, non-flammability, high conductivity, and high thermal stability

allows ILs to be stable and hence, are applicable in various exciting new sensors.^[35,36] Unfortunately, however, the high fluidity of ILs negatively impacts the electrical signal fluctuations when responding to external mechanical deformation on wearable gas-sensing platforms.^[37,38] Previously, we reported solid-state IL devices for gas-sensing induced by the miscibilization of ILs in polymers, which exhibited high stretchability and long-term stability.^[39] However, a limited understanding of the interaction between the target gases and ILs resulted in relatively low sensitivity and selectivity of IL-based gas sensors than those based on semiconducting metal oxides and 2D materials. Also, the realization of skin-attachable gas sensors with 4S has not been well developed.

Herein, we present a stretchable ionotronic gas-sensing sticker (IGS) exhibiting 4S by implementing an IL-based, free-standing solid-state polymer electrolyte (ionic thermoplastic polyurethane, i-TPU) as the sensing channel and inkjet-printed multiwalled carbon nanotubes (MWCNTs) as the electrodes. The patterned electrodes were fabricated using a commercial office inkjet printer with a homogeneous MWCNT conductive ink on a sacrificial polyethylene terephthalate (PET) substrate. The i-TPU free standing and stretchable sensing channel was prepared by the non-covalent association of 1-ethyl-3-methylimidazolium bis(trifluoromethyl-sulfonyl)-imide ([EMIM]⁺[TFSI][−] cation–anion pairs) loaded in the TPU polymer matrix via solution processing. Through the scalable solution process, we successfully fabricated the IGS over a large area (14 in). The IGS showed high sensitivity to NO₂ gas in the order of parts per million (ppm) to parts per billion (ppb). In addition, theoretical density functional theory (DFT) simulation results attributed the high sensitivity and selectivity to the stronger molecular interaction (π -hole receptor effect) between the IL and NO₂ molecules than the interaction between the IL and the other organic gas molecules (toluene, hexane, propanal, ethanol, and acetone). More importantly, the IGS exhibited highly reliable detection of NO₂ after a thermal aging test with 1000 cycles (each cycle from −45 to 125 °C over a period of 30 min), an aging test over 24 h with a high relative humidity (RH) of 85%, and harsh cyclical mechanical bending (up to a radius of curvature of 1 mm) and stretching (up to strain of 50%) deformations. Eventually, we believe that the IGS with 4S properties for reliable signal acquisition will be able to monitor environmentally toxic NO₂ gas in real-life operating environments.

Figure 1a shows a schematic illustration of the fabrication process for the IGS using all-stretchable components, including the solid-state i-TPU sensing channels and inkjet-printed MWCNT electrodes. To realize scaled fabrication, an aqueous, highly conductive MWCNT ink suitable for inkjet printing was prepared. The kinetic ball-milling process was used to reduce the particle size within the homogeneous MWCNT ink to avoid clogging the nozzle of the inkjet printer. Subsequently, to ensure adequate dispersion, the MWCNT ink was mixed in an aqueous suspension with a naphthyl group-based non-ionic surfactant. The printer employed the drop-on-demand method, in which the size and release of an ink drop is well controlled by the piezoelectric force (Figure S1a, Supporting Information).^[40] To realize wearable and stretchable sensing platforms, the MWCNT electrodes should be printed on a flexible PET sacrificial substrate. The interdigitated MWCNT electrodes were

Prof. S. Zhang
State Key Laboratory of Advanced Welding and Joining
Harbin Institute of Technology
Harbin 150001, China

Prof. X. Li
College of Electromechanical Engineering
Qingdao University
Qingdao 266071, China

Prof. A. Fu
College of Chemistry and Chemical Engineering
Qingdao University
Qingdao 266071, China

Dr. C. W. Ahn
Department of Nano-Structured Materials Research
National NanoFab Center (NNFC)
291 Daehak-ro, Yuseong-gu, Daejeon 305–338, Republic of Korea
E-mail: cwahn@nnfc.re.kr

Prof. D. H. Kim
Institute of Nano Science and Technology
Seoul 04763, Republic of Korea

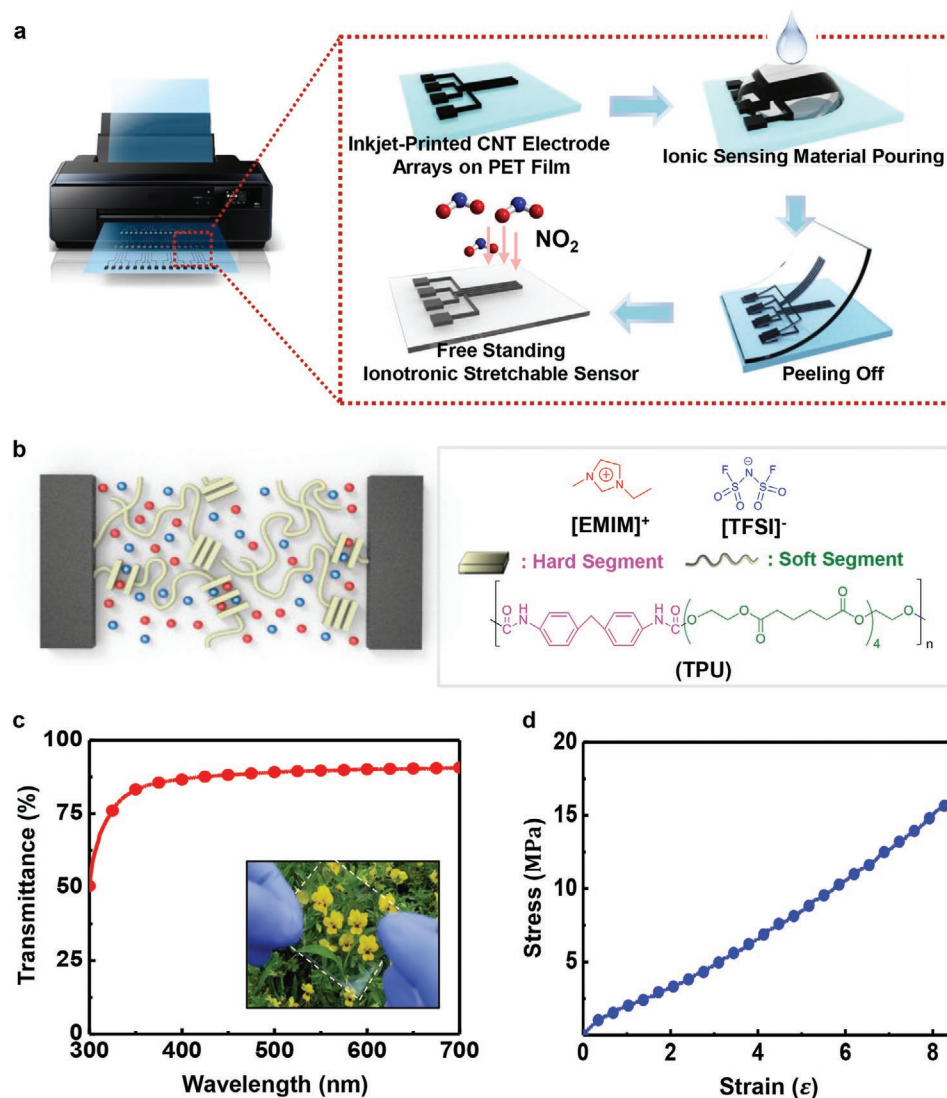


Figure 1. Schematic overview of the ionotronic gas-sensing sticker (IGS). a) Schematic of the fabrication process of the free-standing ionotronic sticker using a commercial inkjet printer. b) Schematics and molecular formula showing the ionic sensing channel of the ionotronic sticker, which is composed of a stretchable matrix (TPU) and an ionic liquid ([EMIM]⁺ and [TFSI]⁻). The red and blue spheres represent the ionic liquid components; [EMIM]⁺ (red) and [TFSI]⁻ (blue). The yellowish polymer matrix (TPU) represents the soft and hard segments forming the blocks. c) Transmittance of the ionic sensing channel. Inset: an image of the hierarchically assembled transparent ionic polymer film. d) Stress-strain curve and the absorption properties of the ionic sensing channel.

highly uniform with a width of 200 μm and were designed by a personal computer (Figure S1b, Supporting Information). The sheet resistance of the MWCNT electrodes was $\approx 2.9 \text{ k}\Omega \text{ sq}^{-1}$, which is sufficient for sensor electrodes (Figure S2, Supporting Information). Detailed information on the preparation and characterization of the MWCNT ink with the inkjet printing process is described in the Experimental Section, Supporting Information (see Figure S3, Supporting Information).

The i-TPU sensing channel was prepared via spin-coating on the surface of the prepatterned MWCNT electrodes, and then detached from the sacrificial substrate for the final IGS fabrication process. The detailed i-TPU fabrication is described in the Experimental Section, Supporting Information. The Raman mapping image (5 $\mu\text{m} \times 5 \mu\text{m}$) of the i-TPU channel reveals

the distribution of ions ([EMIM]⁺[TFSI]⁻) in the TPU matrix (Figure S4, Supporting Information). The Raman peaks of the ILs were centered at 1146 cm^{-1} for the SO_2 symmetric stretching of the anions and at 1433 cm^{-1} for the antisymmetric, C–C, (N) CH_2 , and $\text{CH}_3(\text{N})\text{CN}$ stretching of the cations. These two characteristic peaks do not overlap with those of the TPU matrix (not shown). The TPU has two characteristic peaks for polyester (C=O) and urethane amide (C=O) centered at 1740 cm^{-1} (Table S1, Supporting Information).^[39] The mapping image of the i-TPU shows a uniform intensity ratio of [EMIM]⁺ and [TFSI]⁻ over the entire scanned area, indicating evenly distributed ions in the nanoscale in the TPU matrix. Previously, our group has reported non-covalent interactions between [EMIM]⁺[TFSI]⁻ and the TPU matrix—the ILs served as a plasticizer.^[1,39] Such

interactions resulted in the partial intercalation of ions between hard segments and the binding of ions to soft segments in the TPU, thereby providing a well-mixed state without phase separation (Figure 1b). Finally, as shown in Figure 1c, this enables highly transparent and uniform properties of the hierarchically assembled i-TPU channel (transmittance of 89.7% at 550 nm wavelength).

One of the most important characteristics of flexible devices used in wearable sensors is their mechanical properties. Diverse materials are fabricated with differences of many orders of magnitude in the Young's modulus (E), ranging from liquids (Pa–kPa), elastic materials (MPa), and hard or brittle materials (GPa). In particular, elastic materials can be mechanically compatible with biological tissues.^[41–43] Hence, to investigate the mechanical properties of the solid-state i-TPU film, the stress–strain curve was generated as shown in Figure 1d. The linear behavior without saturation is clearly observed, exhibiting an E of ≈ 2.8 MPa, which is comparable to that of the commonly used polydimethylsiloxane material. Even up to a strain of 600%, degradation behavior was not exhibited. Furthermore, no hysteresis loop of cyclic stress–strain curves was observed, corresponding to 10%, 20%, 30%, and 50% strain, respectively (see Figure S5, Supporting Information). This reflects that the i-TPU film is highly reliable against repeated strains which would be generated by human motion.^[44–46] Eventually, it can be expected that the i-TPU based IGS can be a promising skin-like material, and possesses considerable potential for the realization of skin-attachable electronics.

To observe the gas-sensing capability toward various target analytes, the fabricated IGSs were mounted onto a homemade gas-sensing chamber interconnected with a gas control delivery system and a multiarray data acquisition module (Figure S6, Supporting Information). Nitrogen (N_2) was used as the reference gas, and the total flow rate of gases (N_2 , NO_2 , and volatile organic compounds, VOCs) into the chamber was maintained at 400 sccm during the measurements of the gas response. By using a mass flow controller, Teflon tubing, LOK-type fitting, and valve system, serial gases with exact concentrations were well controlled. The electrical resistances of the channels were monitored as a sensing signal using the data acquisition module. Detailed information on the measurement of the resistance signals is described in the Experimental Section, Supporting Information.

It should be noted that NO_2 gas is very harmful to humans and is classified as an extremely hazardous substance. For example, mild irritation of the nose and throat occurs at 10 ppm of NO_2 exposure, edema occurs at the 25–50 ppm level, and death can occur above 100 ppm due to asphyxiation from fluid in the lungs.^[47] Importantly, there are often no symptoms from exposure other than a transient cough, fatigue, or nausea, but inflammation occurring for hours in the lungs causes edema. Therefore, NO_2 gas was tested as the target analyte to validate the sensing performance of the IGS.

Figure 2a shows the dynamic sensing responses of the IGS at different concentrations of NO_2 gas for room-temperature operations. When NO_2 was introduced into the i-TPU sensing channel, an obvious negative resistance variation was observed. The resistive response ($\Delta R/R_b$) was used to reflect the gas sensitivity. R_b and ΔR represent the baseline of the sensor measured

in a pure N_2 stream and the resistance change resulting from gas exposure, respectively. The resistive response tends to increase as the concentration of NO_2 increased from 250 ppb to 5 ppm. In particular, the limit of detection was found to be down to 250 ppb. The resistive response (reported as a percentage) varied significantly at different concentrations of NO_2 : 0.72% (250 ppb), 2.05% (500 ppb), 14.98% (1 ppm), and 22.59% (5 ppm). These results indicate that highly sensitive resistance variation is capable of detecting gaseous NO_2 in daily life.

To precisely investigate the absorption speed of the NO_2 molecules, the response times, $\tau_{90\%}$ (time taken to achieve 90% of the minimum resistance level), of the ionic sensor versus NO_2 concentrations ranging from 0.25–10 ppm are shown in Figure 2b. Overall, the response time increased from 29–123 s as the concentration of injected NO_2 molecules increase. This indicates that much more time should be taken to dissolve higher concentrations of gas molecules in the IL. Further, the electrical reliability of the resistance variation of the ionic sensor versus time is shown in Figure S7, Supporting Information. With repeated injections of 10 ppm NO_2 , the resistance of the IGS decreased significantly for sensitivity up to 41.5%. Moreover, by purging with a N_2 stream, the resistance recovered to the baseline level. Thus, it can be seen that the IGS with inkjet-printed MWCNT electrodes was stable for certain operation periods without a large drift in the baseline or a reduction in the sensitivity. The highly reliable and sensitive behavior is attributed to the reduction in the viscosity of the IL after being exposed to the gases, resulting in a change in the conductivity of the IL.

In order to confirm the highly selective response to the NO_2 molecules for realizing wearable gas sensors in daily life, we investigated the maximal electrical resistance change ($\Delta R/R_b$)_{max} for various gas molecules: NO_2 , toluene, hexane, propanal, ethanol, and acetone (Figure 2c). During the measurements, the flow concentration of NO_2 into the chamber was maintained at 5 ppm, whereas the other five VOCs were sequentially introduced to the i-TPU sensing channel at a high concentration of 1000 ppm. With such a large difference in concentrations of the NO_2 and VOCs, the low concentration of gaseous NO_2 (5 ppm) revealed a much more sensitive response than the high concentration of VOCs (1000 ppm). The highly sensitive response to the NO_2 molecules is attributed to the greater influence of the interaction between the i-TPU sensing material and the NO_2 gas than with the VOCs. To further confirm the reliability and selectivity of the IGS, the responses to a pure gas (5 ppm NO_2) and mixed gas (5 ppm NO_2 plus 5 ppm toluene) were continuously tested for four cycles (Figure 2d). With the repeated injection of the 5 ppm NO_2 , the sensitivity remained at $\approx 22\%$. A similar sensitivity to the mixed gas was observed; implying that 5 ppm toluene in the NO_2 gas mixture had little effect on the overall sensitivity. Therefore, the IGS could be used as a highly selective NO_2 detector. Moreover, by purging with N_2 , the resistance nearly recovered to the baseline level for each cycle, enabling the IGS to be highly reliable and selective.

The sensing mechanism for the IL-based sensing channel is presented in Figure 3a. The highly viscous characteristic of the IL is derived from the cation–anion interaction. When the IL absorbs gas, the dissolved gas molecules inhibit the ion

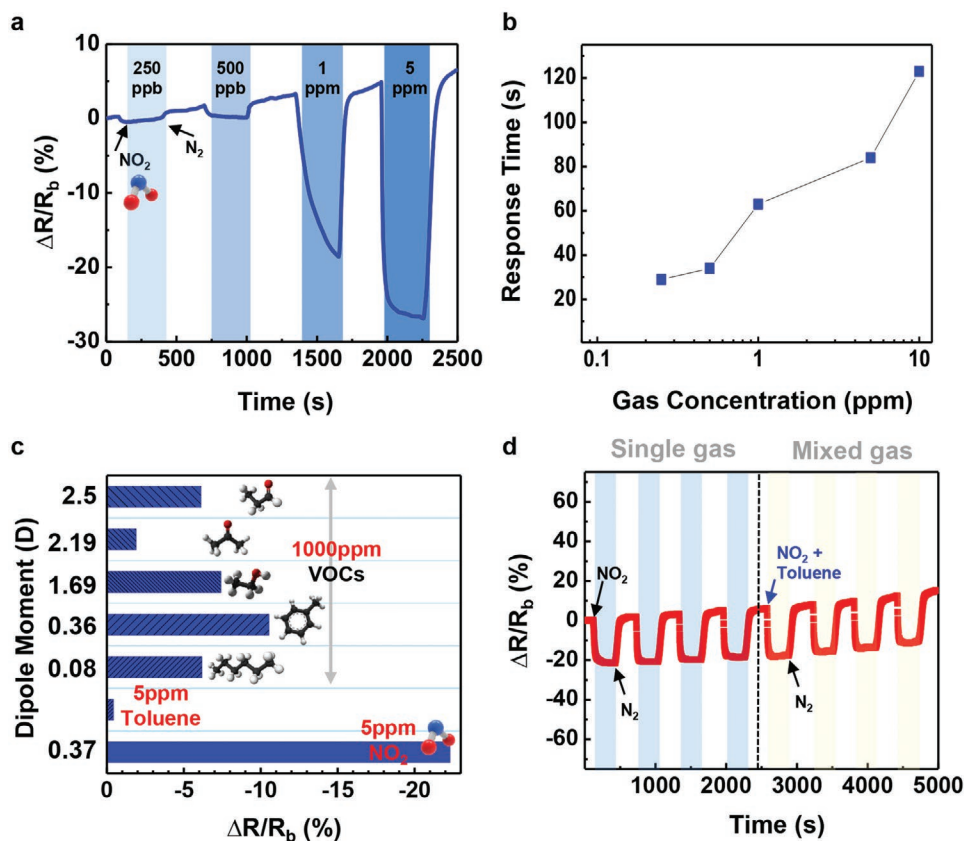


Figure 2. Dynamic gas response of the IGS. a) Transient response–recovery characteristics of the IGS toward the pollutant gas (NO_2) in the concentration range from 0.25 to 5 ppm. b) The response time ($\tau_{90\%}$) of the IGS to different concentrations of NO_2 gas molecules (0.25–5 ppm). c) Selective responses of the IGS toward 5 ppm NO_2 in comparison to those of volatile organic compounds (propanol, acetone, ethanol, toluene, and hexane at 1000 ppm and toluene at 5 ppm) with different dipole moments. d) Reliability and selectivity of the IGS when sequentially exposed to 5 ppm NO_2 for four cycles and to 5 ppm NO_2 mixed with 5 ppm toluene for four cycles.

interaction, resulting in the reduced IL viscosity and leaving an increased number of free ions.^[48] According to Seddon's equation,^[49] the viscosity of ILs after dissolving gas can be described as

$$\eta = \eta_s \exp\left(-\frac{\chi_{cs}}{a}\right) \quad (1)$$

where η_s and η represent the viscosities of the pure $[\text{EMIM}]^+[\text{TFSI}]^-$ IL and gas-dissolved IL at 20 °C, respectively, χ_{cs} is the mole fraction of the gas, and a is a constant for the specific IL. The reduced viscosity of the IL simultaneously leads to increased ion diffusivity and conductivity, which can be explained by the Stokes–Einstein equation:^[50]

$$D = \frac{k_B T}{6\pi\eta r} \quad (2)$$

where D is the diffusion coefficient of the charged ions and η is the viscosity of the IL. Consequently, negative resistance variation signals were observed.

Further, in order to understand the origin of the high sensitivities of the ILs to NO_2 , we performed a quantum chemistry study of the mechanism by which NO_2 was adsorbed by

$[\text{EMIM}]^+[\text{TFSI}]^-$ by employing the Gaussian 09 package.^[50] The Truhlar's M06-2X functional,^[51] which can properly describe the dispersion energies for many non-covalent interaction systems, was selected for the geometry optimization and frequency calculations at the standard 6-31+G(d,p) basis set level. It has been well established that NO_2 can easily dimerize exothermically to form N_2O_4 (with a reaction energy of ≈ -52.5 kJ mol⁻¹ at the M06-2X/6-31+G** level).^[53] Thus, we can assume that a more stable symmetric NO_2 dimer, such as N_2O_4 , may directly participate in the IL adsorption process. Recent work on the highly reversible adsorption of NO_2 in imidazole sulfonate ILs reported by Geng and Wu confirmed the existence of N_2O_4 .^[54] Therefore, in addition to the NO_2 monomer, the interaction mechanism between the ILs and NO_2 dimers was evaluated.

For comparison, the capturing nature of the ILs subjected to toluene was also considered. The electrostatic potential (ESP), which can assist in visualizing the charge distribution at the molecular surface and identify the favorable interaction sites of the adsorbates (NO_2 , N_2O_4 , and toluene), cations, anions, and ion pairs of the ILs, are illustrated in Figure 3b. With respect to the positive and negative regions of the ESPs, the interaction modes between the different species could be probed. For example, the ESPs of the NO_2 and N_2O_4 molecules possessed positive regions above and below the sp^2 -hybridized N atoms,

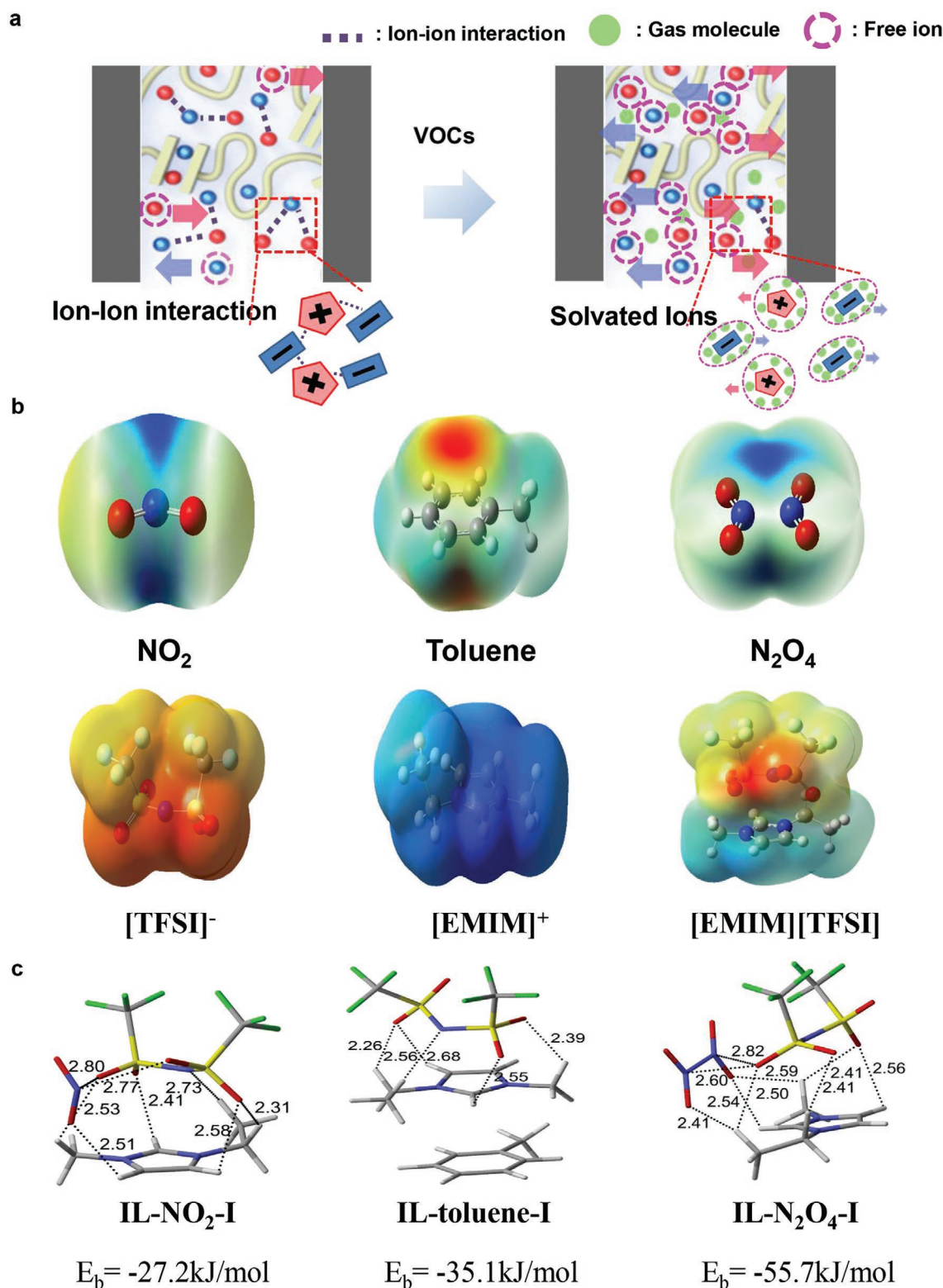


Figure 3. Sensing mechanism and the possible interaction energy of gases with configurations on the $[\text{EMIM}]^+[\text{TFSI}]^-$ ionic liquid using density functional theory (DFT) calculations. a) Schematic illustration of the working mechanism for the IGS. The dashed lines indicate bounded ions due to the ion-ion interaction, and the dashed circles indicate the dissociation of paired ions due to the ion-gas interaction. b) Molecular electrostatic potential surfaces for NO_2 , toluene, N_2O_4 , $[\text{TFSI}]^-$, $[\text{EMIM}]^+$, and $[\text{EMIM}]^+[\text{TFSI}]^-$, where the red and blue colors denote the regions of more negative and more positive charges, respectively. The isodensity contour is 0.0004 electrons per bohr³. c) Optimized structures and binding energies of the most stable interaction modes for $[\text{EMIM}]^+[\text{TFSI}]^-$ - NO_2 , $[\text{EMIM}]^+[\text{TFSI}]^-$ -toluene, and $[\text{EMIM}]^+[\text{TFSI}]^-$ - N_2O_4 at the M06-2X/6-31+G** level.

which have been defined as π -holes by Murray et al.^[55] This positive region can attract the electrons of the O atoms in the TFSI anion and establish the so-called π -hole interactions. Another interaction force arises from the hydrogen bond formed in C–H from the cation and the O atom from NO₂ or N₂O₄. These two types of non-covalent interactions contributed to the stabilization of the NO₂ (N₂O₄)-IL system. In the case of toluene-[EMIM]⁺[TFSI][−], the attraction may be primarily attributed to the π (toluene)– π (imidazolium cation) interactions between the two aromatic rings. Based on the above predictions, the interaction between the anion (or cation) and the adsorbates were considered first to establish the individual energetic contribution to the sensitivity of the ILs to the different adsorbates. The related results of the cation–adsorbate, anion–adsorbate, and the isolated ILs are reported in Figures S8 and S9, Supporting Information. Next, various possible orientations of 1:1 complexes formed between [EMIM]⁺[TFSI][−] and the NO₂, N₂O₄, or toluene molecules were designed, and the optimized structures are presented in Figure S10, Supporting Information. The most stable ones are shown in Figure 3c.

To quantitatively describe the interaction strength between the ILs and adsorbates, the interaction energies were calculated using Equation (3):

$$E_b = E_{\text{IL-adsorbate}} - E_{\text{IL}} - E_{\text{adsorbate}} \quad (3)$$

where $E_{\text{IL-adsorbate}}$, E_{IL} , and $E_{\text{adsorbate}}$ are the energies of the IL–adsorbate complexes, isolated IL, and adsorbate, respectively. As shown in Figure 3b, the calculated binding energies are −272, −35.1, and −55.7 kJ mol^{−1} for the IL–NO₂, IL–toluene, and IL–N₂O₄ complexes, respectively. The order of the interaction strength implies the preferential adsorption of the NO₂ dimer on the ILs, and the observed strong NO₂ sensitivity of the ILs can be reasonably reproduced. Upon further examination of the interaction forces between the N₂O₄ and ILs, the stronger interaction between the N₂O₄ and [EMIM]⁺[TFSI][−] could be understood. NO₂ possesses a four-electron three-center π bond, while N₂O₄ has an eight-electron six-center π bond. The larger delocalized system in the N₂O₄ makes the N–O bond more polarized with a more negative charge on the O and a more positive charge on the N (N₂O₄: N = 0.586, O = −0.293; NO₂: N = 0.554, O = 0.277). Consequently, this change in the electron distribution in the NO₂ dimer than that of the NO₂ monomer results in stronger π -hole (N₂O₄)–LP (O of the TFSI anion) and C–H (imidazolium cation)–O (N₂O₄) hydrogen bond interactions. Furthermore, the strong simultaneous interactions of the N₂O₄ with both the cation and anion of the ILs through a hydrogen bond and π -hole interactions surpass the π – π stacking in the IL–toluene complexes. The atoms in molecules analysis based on the most stable structures shown in Figure S11 and Table S2, Supporting Information, also confirmed the existence and relative strength of the non-covalent interaction forces in [EMIM]⁺[TFSI][−]–NO₂, [EMIM]⁺[TFSI][−]–N₂O₄, and [EMIM]⁺[TFSI][−]–toluene. Therefore, based on the DFT calculations, we can conclude that the high sensitivity to NO₂ by [EMIM]⁺[TFSI][−] arises mainly from the adsorption of the symmetric NO₂ dimer.

Practical wearable sensing requires the devices to be operational even under extreme conditions, including harsh environments and severe mechanical deformations. To investigate the environmental temperature stability of our ionic sensor, we

used the NO₂ pollutant gas at 5 ppm for the thermal cycling test, which was performed by increasing the temperature from −45 to 125 °C in a period 30 min. As shown in Figure 4a, there was no significant degradation in the sensitivity of our device to the NO₂ gas after 250 cycles. Even after 1000 cycles, the magnitude of the response maintained a value similar to that of the raw status. This result indicates that the long-term thermal stability of our ionic sensor can allow the sensor to operate in various temperatures, owing to the intrinsic high thermal stability of each component material (IL, TPU, and MWCNTs).

Moreover, to investigate the environmental humidity effect on the performance of the ionic sensor, a harsh humidity test was conducted. As shown in Figure 4b, after introducing a harsh RH condition of 85% for 24 h, the magnitude of the response to NO₂ was similar to the prestatus level without significant degradation. The long-term environmental humidity stability of the sensor originates from the water resistance of the i-TPU solid electrolyte and the MWCNT electrode. The [EMIM]⁺[TFSI][−] ion pairs have very poor miscibility with water,^[55] and TPU also shows high hydrophobicity.^[56] Therefore, our solid-state i-TPU electrolyte composed of the IL and TPU possessed two properties preventing water penetration. Finally, the high hydrophobicity of the MWCNTs in the electrode of our sensor is beneficial for hydrophobic sensing materials.^[57]

An important trend in wearable sensing electronics is mechanical flexibility, which requires the development of devices that can withstand extremely small bending radii and large tensile strains without any deterioration. Figure 4c shows a photograph of the IGS stuck to the surface of a human arm. As shown in Figure S12a, Supporting Information, the IGS exhibited reasonable adhesion strength toward not only human skin, but also rigid and flexible substrates. Attributing to the stable adhesion property, the IGS displayed high resistance against twisting, compressing, and even stretching deformation of human skin (Figure S12b, Supporting Information). Note that this is a key evidence to demonstrate a superior interfacing stability of the IGS attached to human skin. Also, we conducted a bending stability test by bending the device into different radii. Figure 4d shows the magnitude of the response to the 5 ppm NO₂ pollutant gas after the device was bent with a radius of curvature ranging from 9 to 1 mm. Even when bent to the severe radius of 1 mm, there was no appreciable electrical degradation. To further confirm the stretchable stability of the IGS, we conducted a stretching stability test by stretching the device to different levels of tensile strain. Figure 4e shows the magnitude of the response to the 5 ppm NO₂ pollutant gas after the device was stretched with various strain: 0% strain, 25% strain, and 50% strain, respectively. There was still no significant electrical degradation. It is worth mentioning that the IGS could achieve a stable NO₂ (5 ppm) response even after 300 cycles of extreme mechanical stimuli (bending radius of 1 mm or cyclical straining to 50%), as shown in Figure 4f, while maintaining the sensing capabilities of the IL. Further, surprisingly, the sensing characteristics against 5 ppm NO₂ in the air was maintained even under mechanical deformation (up to stretching state of 50%) (Figure S13, Supporting Information), indicating that the IGS exhibits high reliability that is critically required for wearable gas sensor.

In addition, Figure 5 highlights the ultraperformance of the IGS exhibiting 4S properties compared with the most

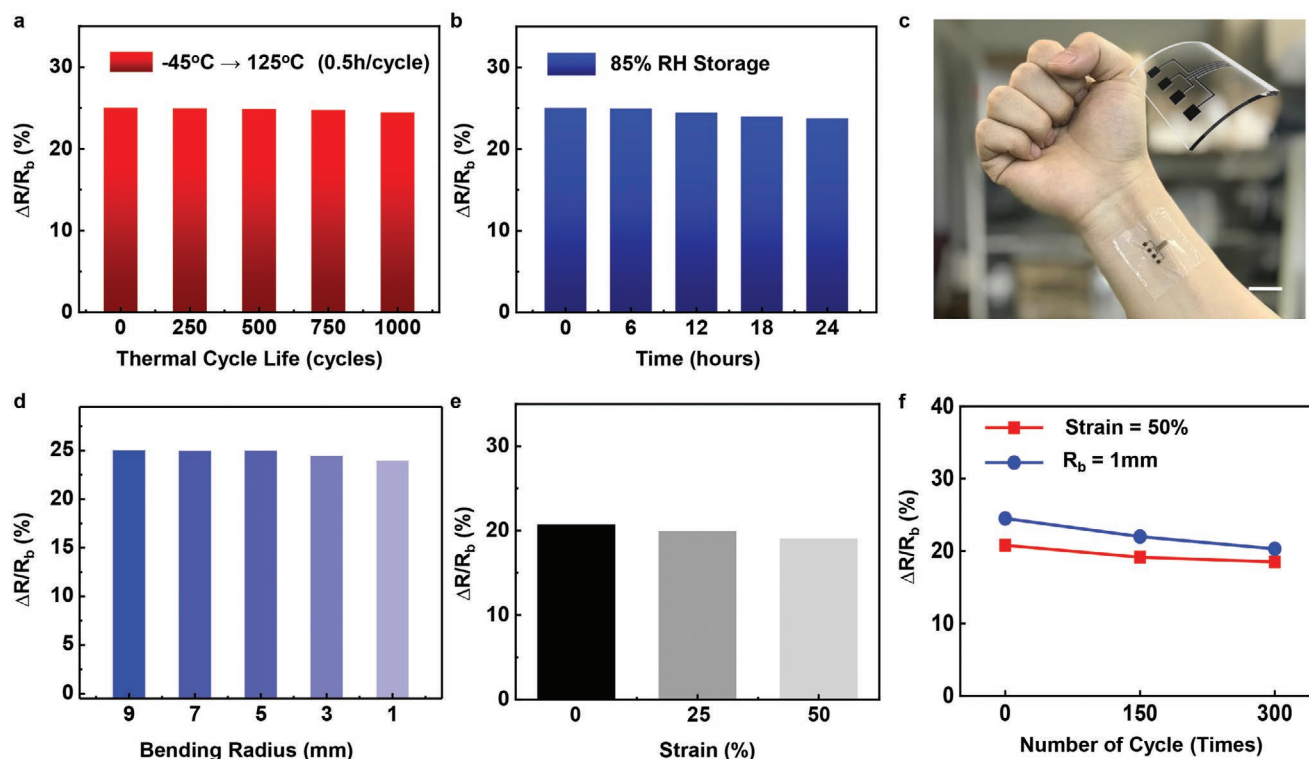


Figure 4. Ultrastable gas (NO_2 at 5 ppm) sensing characteristics of the IGS under various external stimuli. a,b) Stable NO_2 (5 ppm) response of the IGS after: a) thermal aging for 1000 cycles (each cycle from -45 to 125°C for a period of 30 min) and b) exposure to high humidity for 24 h (RH 85%). c) Photograph of the skin-attachable IGS. Scale bar is 5 mm. d) Bending with different bending radii from 9 to 1 mm. e) Stretching with 0%, 25%, and 50% strain, respectively. f) Stable NO_2 (5 ppm) response of the IGS after cyclical bending with a bending radius of 1 mm or cyclical straining at 50%.

sophisticated classes of sensing materials. This work could include all the parameter points and cover most of the space in red. This implies that the IGS satisfies the primary 4S parameters. The details of other materials are shown in Table S3, Supporting Information. Therefore, it can be noted that the ultrastable IGS device designed by us is potentially more valuable for use in skin-attachable sensors than other high E -fragile sensing materials, such as 2D materials and metal oxides.

In summary, a scalable, stretchable IGS with superior chemical sensing performance was developed. The IGS was fabricated by implementing the solid-state i-TPU sensing

material and inkjet-printed MWCNT electrodes. In particular, the IGS suggested by us exhibited high sensitivity and selectivity to toxic NO_2 gas molecules with a broad detection range of concentrations from ppm to ppb, and it remained operational after experiencing harsh environmental conditions of high temperature and humidity. Moreover, the IGS retained the capability of sensing pollutant molecules after experiencing mechanical deformations through bending and stretching. This enables practical applications for wearable gas sensors. Furthermore, the fabrication of the materials by printing technology and all-solution processing introduces a high-efficiency and low-cost method to scale commercial production in the field of wearable sensing electronics. We believe that the practical parameters for the application of the concept presented here can be useful for other ionotronic sensing materials.

Supporting Information

Supporting Information is available from the Wiley Online Library or from the author.

Acknowledgements

M.L.J., S.P., and H.K contributed equally to this work. This work was financially supported by the Young Taishan Scholars Program of Shandong Province (grand nos. 201909099), the National Natural Science Foundation of China (grand nos. 52003134), and the Research

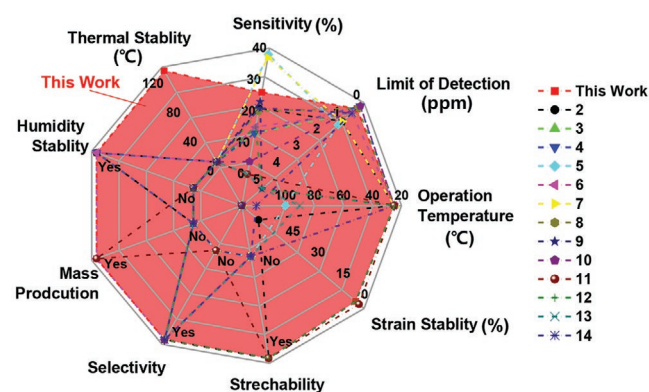


Figure 5. The figure of merit for the IGS compared to reported NO_2 gas sensor researches.

Start-up Foundation of Qingdao University. The work was also supported by the Global Research Development Center Program (2015K1A4A3047100, FIRST Nano Co-op Center, NNFC) and the Basic Science Research Program (2020R1A2C3014237, 2017R1A5A1015596, and 2018R1A2B3008658) of the National Research Foundation of Korea funded by the Ministry of Science, ICT. The authors thank Prof. Shuzhi Sam Ge for supporting the experimental work with funding from "One Case, One Discussion" for Top Talents of Shandong Province. The demonstration in Figure 4c showing adhesion to skin did not require ethical approval. The human volunteer, who was one of the authors of this article, took part with informed consent, following consideration of any risks involved.

Conflict of Interest

The authors declare no conflict of interest.

Data Availability Statement

The data that support the findings of this study are available from the corresponding author upon reasonable request.

Keywords

chemical sensing, ionotronic skin, π -hole receptor effect, skin-attachable gas sensors

Received: November 8, 2020

Revised: December 27, 2020

Published online: February 17, 2021

- [1] M. L. Jin, S. Park, Y. Lee, J. H. Lee, J. Chung, J. S. Kim, J. S. Kim, S. Y. Kim, E. Jee, D. W. Kim, J. W. Chung, S. G. Lee, D. Choi, H. T. Jung, D. H. Kim, *Adv. Mater.* **2017**, 29, 1605973.
- [2] A. Chortos, J. Liu, Z. Bao, *Nat. Mater.* **2016**, 15, 937.
- [3] S. K. Kang, R. K. Murphy, S. W. Hwang, S. M. Lee, D. V. Harburg, N. A. Krueger, J. Shin, P. Gamble, H. Cheng, S. Yu, Z. Liu, J. G. McCall, M. Stephen, H. Ying, J. Kim, G. Park, R. C. Webb, C. H. Lee, S. Chung, D. S. Wie, A. D. Gujar, B. Vernulapalli, A. H. Kim, K. M. Lee, J. Cheng, Y. Huang, S. H. Lee, P. V. Braun, W. Z. Ray, J. A. Rogers, *Nature* **2016**, 530, 71.
- [4] M. L. Hammock, A. Chortos, B. C. Tee, J. B. Tok, Z. Bao, *Adv. Mater.* **2013**, 25, 5997.
- [5] World Health Organization, *Global Health Risks: Mortality and Burden of Disease Attributable to Selected Major Risk*, World Health Organization, Switzerland **2009**; https://www.who.int/healthinfo/global_burden_disease/GlobalHealthRisks_report_full.pdf (accessed: November 2020).
- [6] L. Lamsal, R. Martin, D. Parrish, N. Krotkov, *Environ. Sci. Technol.* **2013**, 47, 7855.
- [7] M. J. Nieuwenhuijsen, *Environ. Health* **2016**, 15, 161.
- [8] Y. S. Rim, S. H. Bae, H. Chen, N. De Marco, Y. Yang, *Adv. Mater.* **2016**, 28, 4415.
- [9] H. Haick, Y. Y. Broza, P. Mochalski, V. Ruzsanyi, A. Amann, *Chem. Soc. Rev.* **2014**, 43, 1423.
- [10] F. Favier, E. C. Walter, M. P. Zach, T. Benter, R. M. Penner, *Science* **2001**, 293, 2227.
- [11] B. Buszewski, A. Ulanowska, T. Ligor, N. Denderz, A. Amann, *Biomed. Chromatogr.* **2009**, 23, 551.
- [12] C. Turner, P. Španěl, D. Smith, *Rapid Commun. Mass Spectrom.* **2006**, 20, 61.
- [13] J. W. Grate, S. L. Rose-Pehrsson, D. L. Venezky, M. Klusty, H. Wohltjen, *Anal. Chem.* **1993**, 65, 1868.
- [14] C. Di Natale, A. Macagnano, E. Martinelli, R. Paolesse, G. D'Arcangelo, C. Roscioni, A. Finazzi-Agro, A. D'Amico, *Biosens. Bioelectron.* **2003**, 18, 1209.
- [15] I.-D. Kim, A. Rothschild, B. H. Lee, D. Y. Kim, S. M. Jo, H. L. Tuller, *Nano Lett.* **2006**, 6, 2009.
- [16] G. Peng, U. Tisch, O. Adams, M. Hakim, N. Shehada, Y. Y. Broza, S. Billan, R. Abdah-Bortnyak, A. Kuten, H. Haick, *Nat. Nanotechnol.* **2009**, 4, 669.
- [17] F. J. Ibañez, F. P. Zamborini, *Small* **2012**, 8, 174.
- [18] H. Jin, T.-P. Huynh, H. Haick, *Nano Lett.* **2016**, 16, 4194.
- [19] H.-W. Yoo, S.-Y. Cho, H.-J. Jeon, H.-T. Jung, *Anal. Chem.* **2015**, 87, 1480.
- [20] U. Lange, V. M. Mirsky, *Anal. Chim. Acta* **2011**, 687, 105.
- [21] L. K. Randeniya, P. J. Martin, A. Bendavid, J. McDonnell, *Carbon* **2011**, 49, 5265.
- [22] F. Schedin, A. K. Geim, S. V. Morozov, E. Hill, P. Blake, M. Katsnelson, K. S. Novoselov, *Nat. Mater.* **2007**, 6, 652.
- [23] J.-S. Kim, H.-W. Yoo, H. O. Choi, H.-T. Jung, *Nano Lett.* **2014**, 14, 5941.
- [24] S.-Y. Cho, H.-J. Koh, H.-W. Yoo, J.-S. Kim, H.-T. Jung, *ACS Sens.* **2017**, 2, 183.
- [25] S.-Y. Cho, H.-W. Yoo, J. Y. Kim, W.-B. Jung, M. L. Jin, J.-S. Kim, H.-J. Jeon, H.-T. Jung, *Nano Lett.* **2016**, 16, 4508.
- [26] G. Katwal, M. Paulose, I. A. Rusakova, J. E. Martinez, O. K. Varghese, *Nano Lett.* **2016**, 16, 3014.
- [27] G. F. Fine, L. M. Cavanagh, A. Afonja, R. Binions, *Sensors* **2010**, 10, 5469.
- [28] T. Akamatsu, T. Itoh, N. Izu, W. Shin, *Sensors* **2013**, 13, 12467.
- [29] J. D. Fowler, M. J. Allen, V. C. Tung, Y. Yang, R. B. Kaner, B. H. Weiller, *ACS Nano* **2009**, 3, 301.
- [30] S.-Y. Cho, S. J. Kim, Y. Lee, J.-S. Kim, W.-B. Jung, H.-W. Yoo, J. Kim, H.-T. Jung, *ACS Nano* **2015**, 9, 9314.
- [31] S. Y. Cho, Y. Lee, H. J. Koh, H. Jung, J. S. Kim, H. W. Yoo, J. Kim, H. T. Jung, *Adv. Mater.* **2016**, 28, 7020.
- [32] S.-Y. Cho, H.-J. Koh, H.-W. Yoo, H.-T. Jung, *Chem. Mater.* **2017**, 29, 7197.
- [33] S. J. Kim, H.-J. Koh, C. E. Ren, O. Kwon, K. Maleski, S.-Y. Cho, B. Anasori, C.-K. Kim, Y.-K. Choi, J. Kim, *ACS Nano* **2018**, 12, 986.
- [34] Z. Lei, B. Chen, Y.-M. Koo, D. R. MacFarlane, *Chem. Rev.* **2017**, 117, 6633.
- [35] J. L. Bideau, L. Viau, A. Vioux, *Chem. Soc. Rev.* **2011**, 40, 907.
- [36] P. Hapiot, C. Lagrost, *Chem. Rev.* **2008**, 108, 2238.
- [37] A. Rehman, X. Zeng, *RSC Adv.* **2015**, 5, 58371.
- [38] I. Krossing, J. M. Slattery, C. Dague, P. J. Dyson, A. Oleinikova, H. Weingärtner, *J. Am. Chem. Soc.* **2006**, 128, 13427.
- [39] M. L. Jin, S. Park, J. S. Kim, S. H. Kwon, S. Zhang, M. S. Yoo, S. Jang, H. J. Koh, S. Y. Cho, S. Y. Kim, *Adv. Mater.* **2018**, 30, 1706851.
- [40] O.-S. Kwon, H. Kim, H. Ko, J. Lee, B. Lee, C.-H. Jung, J.-H. Choi, K. Shin, *Carbon* **2013**, 58, 116.
- [41] S. Wagner, S. Bauer, *MRS Bull.* **2012**, 37, 207.
- [42] J. Xu, S. Wang, G.-J. N. Wang, C. Zhu, S. Luo, L. Jin, X. Gu, S. Chen, V. R. Feig, J. W. To, *Science* **2017**, 355, 59.
- [43] S. Wang, J. Xu, W. Wang, G.-J. N. Wang, R. Rastak, F. Molina-Lopez, J. W. Chung, S. Niu, V. R. Feig, J. Lopez, *Nature* **2018**, 555, 83.
- [44] H. Wu, G. Yang, K. Zhu, S. Liu, W. Guo, Z. Jiang, Z. Li, *Adv. Sci.* **2020**, 8, 2001938.
- [45] B. Ying, Q. Wu, J. Li, X. Liu, *Mater. Horiz.* **2020**, 7, 477.
- [46] T. Yamada, Y. Hayamizu, Y. Yamamoto, Y. Yomogida, A. Izadi-Najafabadi, D. N. Futaba, K. Hata, *Nat. Nanotechnol.* **2011**, 6, 296.
- [47] Medical Management Guidelines for Nitrogen Oxides, <https://www.atsdr.cdc.gov/mmg/mmg.asp?id=394&tid=69> (accessed: November 2020).
- [48] Z. X. Zhu, H. Zhang, J. Wu, *Sens. Actuators, B* **2014**, 202, 105.

- [49] K. R. Seddon, A. Stark, M.-J. Torres, *Pure Appl. Chem.* **2000**, 72, 2275.
- [50] M. J. Frisch, G. W. Trucks, H. B. Schlegel, G. E. Scuseria, M. A. Robb, J. R. Cheeseman, G. Scalmani, V. Barone, B. Mennucci, G. A. Petersson, H. Nakatsuji, M. Caricato, X. Li, H. P. Hratchian, A. F. Izmaylov, J. Bloino, G. Zheng, J. L. Sonnenberg, M. Hada, M. Ehara, K. Toyota, R. Fukuda, J. Hasegawa, M. Ishida, T. Nakajima, Y. Honda, O. Kitao, H. Nakai, T. Vreven, J. A. Montgomery Jr., J. E. Peralta, F. Ogliaro, M. Bearpark, J. J. Heyd, E. Brothers, K. N. Kudin, V. N. Staroverov, T. Keith, R. Kobayashi, J. Normand, K. Raghavachari, A. Rendell, J. C. Burant, S. S. Iyengar, J. Tomasi, M. Cossi, N. Rega, J. M. Millam, M. Klene, J. E. Knox, J. B. Cross, V. Bakken, C. Adamo, J. Jaramillo, R. Gomperts, R. E. Stratmann, O. Yazyev, A. J. Austin, R. Cammi, C. Pomelli, J. W. Ochterski, R. L. Martin, K. Morokuma, V. G. Zakrzewski, G. A. Voth, P. Salvador, J. J. Dannenberg, S. Dapprich, A. D. Daniels, O. Farkas, J. B. Foresman, J. V. Ortiz, J. Cioslowski, D. J. Fox, *Gaussian 09, Revision C.01*, Gaussian, Inc., Wallingford CT, USA **2010**.
- [51] Y. Zhao, D. G. Truhlar, *Theor. Chem. Acc.* **2008**, 120, 215.
- [52] W.-G. Liu, W. A. Goddard III, *J. Am. Chem. Soc.* **2012**, 134, 12970.
- [53] G. Yuan, F. Zhang, J. Geng, Y.-T. Wu, *RSC Adv.* **2014**, 4, 39572.
- [54] J. S. Murray, P. Lane, T. Clark, K. E. Riley, P. Politzer, *J. Mol. Model.* **2012**, 18, 541.
- [55] J. Ranke, A. Othman, P. Fan, A. Müller, *Int. J. Mol. Sci.* **2009**, 10, 1271.
- [56] K. Matsunaga, K. Sato, M. Tajima, Y. Yoshida, *Polym. J.* **2005**, 37, 413.
- [57] K. A. Wepasnick, B. A. Smith, K. E. Schrote, H. K. Wilson, S. R. Diegelmann, D. H. Fairbrother, *Carbon* **2011**, 49, 24.